Environmental Science & Technology

Article

pubs.acs.org/est

Extracellular Saccharide-Mediated Reduction of Au^{3+} to Gold Nanoparticles: New Insights for Heavy Metals Biomineralization on Microbial Surfaces

Fuxing Kang,[‡,§] Xiaolei Qu,[§] Pedro J. J. Alvarez,[#] and Dongqiang Zhu*[,†]

[†]School of Urban and Environmental Sciences, Peking University, Beijing 100871, China

[‡]College of Resources and Environmental Sciences, Nanjing Agricultural University, Jiangsu 210095, China

[§]State Key Laboratory of Pollution Control and Resource Reuse/School of the Environment, Nanjing University, Jiangsu 210046, China

[#]Department of Civil and Environmental Engineering, Rice University, Houston Texas 77005, United States

Supporting Information

ABSTRACT: Biomineralization is a critical process controlling the biogeochemical cycling, fate, and potential environmental impacts of heavy metals. Despite the indispensability of extracellular polymeric substances (EPS) to microbial life and their ubiquity in soil and aquatic environments, the role played by EPS in the transformation and biomineralization of heavy metals is not well understood. Here, we used gold ion (Au^{3+}) as a model heavy metal ion to quantitatively assess the role of EPS in biomineralization and discern the responsible functional groups. Integrated spectroscopic analyses showed that $Au^{3+}$was readily reduced to zerovalent gold nanoparticles (AuNPs, 2−15 nm in size) in aqueous suspension of *Escherichia coli* or dissolved EPS extracted from microbes. The majority of AuNPs (95.2%) was formed outside *Escherichia coli* cells, and the removal of EPS attached to cells pronouncedly suppressed Au^{3+} reduction, reflecting the predominance of the extracellular matrix in Au^{3+} reduction. XPS, UV−vis, and FTIR analyses corroborated that Au^{3+} reduction was mediated by the hemiacetal groups (aldehyde equivalents) of reducing saccharides of EPS. Consistently, the kinetics of AuNP formation obeyed pseudo-second-order reaction kinetics with respect to the concentrations of Au^{3+} and the hemiacetal groups in EPS, with minimal dependency on the source of microbial EPS. Our findings indicate a previously overlooked, universally significant contribution of EPS to the reduction, mineralization, and potential detoxification of metal species with high oxidation state.

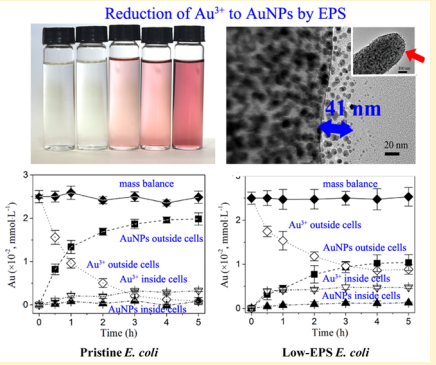

INTRODUCTION

Microorganisms are major players in metal cycling and mineral formation (e.g., biomineralization) in various environments.[1,2] Bacteria are known to use endoenzymes, extracellular enzymes, or exogenous oxidants and reductants to reduce/oxidize essential metals (e.g., iron and manganese[3]) and heavy metals of environmental concern (e.g., uranium,[4] chromium,[5] and arsenic[6]), effectively mediating their biogeochemical cycling and environmental fate.[7,8]

Microorganisms can secrete and embed themselves in extracellular polymeric substances (EPS) that are comprised mostly of polysaccharides and proteins.[9,10] EPS are a major component of biofilms and play a key role in cell surface attachment and microhabitat formation to protect cells from environmental stresses such as desiccation, predation, antibiotic agents, high salinity, and extreme temperature and pH conditions.[11,12] A number of studies have been dedicated to understanding the organic molecules and functional groups in EPS that may control extracellular biomineralization of heavy/transition metals and associated biological and toxic effects. The large content of chelating groups (e.g., amino, thiol, carboxyl, and phenol) in EPS are known to bind and effectively immobilize heavy metal ions (such as Cd^{2+}, Pb^{2+}, and Zn^{2+}) within the extracellular matrix, leading to attenuated toxicity.[13,14] Extracellular polysaccharides can template assembly of iron oxyhydroxide (FeOOH) nanofibers in proximity to the cell membrane to harness the proton gradient for energy generation.[15] Similarly, it was proposed that the strong association of peptide-rich organic matter with biogenic nano metal-sulfides (e.g., ZnS) serves as an important means of extracellular biomineralization through limiting the dispersal of the nanoparticles.[16]

EPS were reported to facilitate the reduction of high-oxidation-state metals such as U(VI) and Cr(VI), which are subsequently immobilized on the surfaces of microorganisms,[17,18] although the underlying reduction mechanisms are not well understood. We recently reported that saccharides in

Received: November 23, 2016
Revised: January 31, 2017
Accepted: February 2, 2017
Published: February 2, 2017

DOI: 10.1021/acs.est.6b05930
Environ. Sci. Technol. 2017, 51, 2776−2785

EPS can reduce silver ions (Ag^+) to zerovalent silver nanoparticles (AgNPs), and act as a permeable barrier to attenuate the toxicity of Ag^+.[19] Whereas this reductive process may represent an important mechanism for microbial defense against some toxic metal ions, its environmental significance for metal biogeochemistry may be greater since EPS are ubiquitous in the environment. This underscores the need to advance our quantitative understanding of the relationship between reducing functional groups in EPS saccharides from various microbial sources and metal biomineralization patterns. EPS also represent an essential pool of labile natural organic carbon, and are known to be the major component of biofilms which represent a dominant form of microbial existence. For example, EPS can also be released in the dissolved form, representing an essential pool (up to 50%) of labile and semilabile dissolved organic matter (DOM) in natural waters.[11] Therefore, EPS have a broader environmental and ecological significance.

Gold (Au) is a rare, inert, and nonessential element to microorganisms; however, zerovalent gold nanoparticles (AuNPs) are considered as promising candidates for many new nanoenabled applications in optics, electronics, and catalysis, owing to their unique shape, size, and crystal structure arrangement.[20] Biosynthesis of AuNPs using microbes and plant species has drawn increasing attention.[21−24] Some microorganisms such as *Thermomonospora* sp.[25] and *Fusarium oxysporum*[26] were found to utilize autologous secretions to synthesize AuNPs in extracellular matrices. The extracellular enzymes[27] and thiol groups in plant proteins[28] were proposed to be responsible for the reduction of gold ion. Reduction of gold ion to AuNPs by extracellular biopolymers (such as delftibactin and thiol-peptides) can protect against toxicity of gold ion and result in gold biomineralization.[29,30] Notably, the reduction of gold ion to zerovalent gold is a unidirectional transformation.[31,32] The irreversible reduction property of gold ion makes it a convenient model system to identify the molecular origin of the reducing power of biomacromolecules (such as EPS) and their potential role played in redox transformation of heavy metals.

In the present study, we propose a new mechanism to address the environmental significance of microbial EPS in the redox cycling and biomineralization of heavy metals. Using Au^{3+} as a model oxidized metal and integrated spectroscopic techniques, we quantitatively assess the reducing capability of EPS from various microbial sources and discern the functional groups responsible for the reductive formation of AuNPs.

MATERIALS AND METHODS

Materials. Chloroauric acid (>99.8%), silver nitrate (>99.0%), sodium chloride (>99.0%), D-glucose (>99.5%), and potassium iodide (>99.0%) were purchased from Sigma-Aldrich (St. Louis, MO). Peptone and yeast extract in biotechnology grade were purchased from Oxoid Co., Ltd. (England). Ammonium hydroxide (26%, w/v), sodium hydroxide (>96%), and hydrochloric acid (36%, w/v) were from Sinopharm Chemical Reagent Co., Ltd. (China). Purified bacterial extracellular lipopolysaccharides (>99%) extracted from EPS of *Escherichia coli* were purchased from Sigma-Aldrich. The tested lipopolysaccharides are important constituents of EPS, and are protein-free, which facilitates demonstrating that thiol-bearing proteins are not a prerequisite for Au^{3+} reduction. According to the information provided by the vendor, the lipopolysacchrides are composed of C (70.0%), O (16.1%), H (11.3%), N (2.5%), and trace P (<0.1%) and S (<0.08%). Ultrapure water (18.2 MΩ·cm) was produced by a Milli-Q system (Millipore, Bedford, MA).

Extraction and Characterization of EPS. Dissolved EPS were prepared using a chemical free, sonication-based method as previously described.[19,33] Briefly, Gram-negative *E. coli* (DH5α) were cultured in 20 mL of LB (Luria−Bertani) medium (comprising 10 $g{\cdot}L^{-1}$ peptone, 5 $g{\cdot}L^{-1}$ yeast extract, and 10 $g{\cdot}L^{-1}$ NaCl) at 37 °C for 6 h, and then transferred into 1 L of fresh LB medium and cultured for another 48 h to reach a stable phase. The bacteria were separated from the LB medium by centrifugation (6000*g*, 4 °C), followed by repeated washing with Milli-Q water and centrifugation until a negative chloride testing on the supernatant by $AgNO_3$. The obtained cell pellets were resuspended with Milli-Q water (approximately 9×10^{12} cells$\cdot L^{-1}$). The suspension was sonicated with an intensity of 2.7 $W{\cdot}cm^2$ and a frequency of 40 kHz at 4 °C for 10 min to separate EPS from *E. coli*, and immediately centrifuged at 11 000*g* and 4 °C for 20 min to remove the cells. The supernatant was collected and filtered through a 0.22 μm membrane (Anpel). The resulting filtrate containing dissolved EPS (32.8 $mg{\cdot}L^{-1}$ on a dry weight basis) was stored at 4 °C for future experiments.

Total organic carbon (TOC) content of EPS solution was measured by a TOC-5000A (Shimadzu, Kyoto, Japan). Contents of proteins (112.8 $mg{\cdot}g^{-1}$), saccharides (326.7 $mg{\cdot}g^{-1}$), humic-like substance (6.13 $mg{\cdot}g^{-1}$), and nucleic acids (0.33 $mg{\cdot}g^{-1}$) in the EPS from *E. coli* were determined according to previous studies.[34−36] The nucleic acid concentration in EPS was very low, indicating negligible cell lysis during EPS extraction. To test the microbial source-dependence of EPS and assess how generalizable the reducing reaction is, Gram-positive *Bacillus subtilis* and fungal *Saccharomyces cerevisiae* were also used as additional sources for EPS extraction. The culture mediums for *B. subtilis* and *S. cerevisiae* were LB and SPM (synthetic potato medium, comprising 20% potato juice, 20 $g{\cdot}L^{-1}$ sucrose, 3 $g{\cdot}L^{-1}$ KH_2PO_4, 1.5 $g{\cdot}L^{-1}$ $MgSO_4$, and 10 $mg{\cdot}L^{-1}$ vitamin B with a pH of 6.0), respectively. The EPS were extracted using the same method as described for *E. coli*.

Determination of Hemiacetal Groups in EPS. Tollens' reagent was used to characterize the hemiacetal groups in reducing saccharides.[37−39] The cyclic hemiacetal associated with the side chain and/or end group in reducing saccharides would spontaneously open up and change into the aldehyde-bearing linear structure when reacting with the oxidizing agent (Tollens' reagent). Specifically, Tollens' reagent ($Ag(NH_3)_2OH$) was prepared by gradually dropping an aqueous ammonia solution (5%, w/v) into a clean glass tube containing 1 mL of aqueous $AgNO_3$ solution (2%, w/v) until the precipitate just dissolved. Three different EPS (10 mL, 32.8 $mg{\cdot}L^{-1}$), each extracted from an individual microbial species (*E. coli*, *B. subtilis*, or *S. cerevisiae*), were mixed with 1 mL of Tollens' reagent, respectively. The mixtures were water bathed for 10 min at 50 °C, followed by adjusting pH to 4.0 in order to turn the unreacted $Ag(NH_3)_2OH$ into Ag^+. The produced Ag^+ was titrated using an autotitrator (WDDY-2008J, Datang, China) equipped with a silver ion-selectivity electrode (Pag/S-1−01, INESA, China) and a mercurous sulfate reference electrode (C−K_2SO_4-1, INESA, China). The titration was performed using 0.1 $mmol{\cdot}L^{-1}$ NaCl with a speed of 10 μL per 20 s at 30 °C and 150 rpm magnetic stirring. The titration curves are shown in Supporting Information (SI) Figure S1.

Reaction of Tollens' reagent with reducing saccharides,

DOI: 10.1021/acs.est.6b05930
Environ. Sci. Technol. 2017, 51, 2776−2785

$$[RCHO] + 2Ag(NH_3)_2OH \rightarrow [RCOONH_4] + 2Ag\downarrow + 3NH_3\uparrow + H_2O \quad (1)$$

Ag^+ releases in acidic condition,

$$Ag(NH_3)_2OH + 3H^+ = 2NH_4^+ + Ag^+ + H_2O \quad (2)$$

Released Ag^+ titrated by Cl^-,

$$Ag^+ + Cl^- = AgCl\downarrow \quad (3)$$

The molarity of Ag^+ reacted with reducing saccharides can be calculated as follows,

$$[\text{reacting } Ag^+ \text{with reducing saccharides}] = [\text{initial } Ag^+] - [\text{titrated } Ag^+ \text{by } Cl^-] \quad (4)$$

According to eqs 1 and 2, the molarity of hemiacetal groups (aldehyde equivalents) of reducing saccharides in EPS can be calculated as follows,

$$[\text{molarity of reducing saccharides in EPS}] = [\text{reacting } Ag^+ \text{with reducing saccharides}]/2 \quad (5)$$

The content of hemiacetal groups in EPS was determined to be 1.26 mmol·g^{-1} (on a dry weight basis) for *E. coli* EPS, 1.77 mmol·g^{-1} for *B. subtilis* EPS, and 1.77 mmol·g^{-1} for *S. cerevisiae* EPS. The content of hemiacetal groups in purified extracellular lipopolysaccharides was determined to be 0.35 mmol·g^{-1} using the same method.

Reduction of Au^{3+} to AuNPs in the Presence of *E. coli* or Aqueous Dissolved EPS. *E. coli* cells (48 h growth to a stable phase[19]) were separated from LB medium by centrifugation (6000*g*, 4 °C), washed with Milli-Q water for three times, and resuspended in 19.8 mL Milli-Q water with pH preadjusted to 8.5. Then 200 μL of Au^{3+} stock solution (51.5 mmol·L^{-1}) was added to obtain 20 mL of solution containing 0.515 mmol·L^{-1} Au^{3+} and 9×10^{12} cells·L^{-1}. After mixing, the pH was stable at 7.2 ± 0.4. All reduction experiments were conducted in the dark for 6 h at 30 ± 0.5 °C.

In addition, the kinetics of AuNP formation in the presence of EPS or lipopolysaccharides was examined by a similar set of experiments, except that the *E. coli* suspension was replaced by aqueous dissolved EPS or lipopolysaccharides. Au^{3+} reduction kinetics in EPS solutions extracted from *E. coli*, *B. subtilis*, and *S. cerevisiae*is was tested separately at single-point initial concentrations of reactants. After mixing aqueous EPS (32.8 mg·L^{-1}) with Au^{3+} (0.515 mmol·L^{-1}), the samples (pH 7.2) were manually shaken for approximately 10 s, and added into a quartz cuvette with an optical path of 1 cm. The absorption spectra were recorded every 2.0 min at a wavelength range of 200−800 nm by a Cary 50 UV−vis spectrophotometer (Varian). Control reactions included 0.515 mmol·L^{-1} uninoculated chloroauric acid prepared with Milli-Q water. A separate set of experiments was conducted to determine the effects of pH (5, 6, 8, and 9, adjusted with HCl or NaOH) on the reaction kinetics of AuNP formation in the presence of *E. coli* EPS. At least 150 data points were collected for each reaction kinetic curve, and the reaction rate constant was obtained by linear regression and reported as mean ± standard deviation.

Mass Distribution of Au^{3+} and AuNPs Inside and Outside Cells. The fate of gold was determined in the presence of *E. coli* cells under two different EPS conditions: without manipulation of EPS (referred as pristine cells) and with removal of EPS using above-mentioned sonication/centrifugation method (referred as low-EPS cells). Stock solution of Au^{3+} was added to *E. coli* water suspension in a 40 mL glass vial to obtain solution containing 2.5×10^{-2} mmol·L^{-1} Au^{3+} and 9×10^{12} cells·L^{-1}. The samples were incubated and shaken in an orbital shaker in the dark at 30 ± 0.5 °C, and a subset of samples was sacrificed at desired time intervals for analysis to detect concentrations of Au^+ and AuNPs inside cells and outside cells (i.e., in water and in extracellular matrix). After centrifugation (6000*g* at 4 °C for 10 min), the supernatant was withdrawn and stored in the dark at 4 °C, and the cell pellets were resuspended with Milli-Q water. Then EPS were extracted from the bacterial suspension using the sonication/centrifugation method as mentioned above. The supernatant containing aqueous EPS was filtered through a 0.45 μm membrane to remove unsettled cells. The filtered cells on the membrane were resuspended in Milli-Q water and filtered. Such process was repeated at least five times to make sure that EPS and associated gold contents sorbed to cells were completely washed out (verified by nondetectable gold content in the final filtrate after microwave digestion). The filtrates were collected and merged with the respective supernatant for analysis of Au^{3+} and AuNPs using the cloud point extraction (CPE) method as described in our previous study.[19] After the removal of EPS and associated gold contents, the remaining cell pellets were disrupted by high intensive focused ultrasound (HIFU) (Φ6, Scientz, China) with an intensity of 450 W·cm^2 and a frequency of 24 kHz at 0 °C for 5 min. No bacterial colonies were observed in the plate test (15 g·L^{-1} agar in chloride-free medium), suggesting that the *E. coli* cells were completely disrupted. The cell lysate was collected and analyzed for the concentrations of Au^{3+} and AuNPs using the CPE method. Triplicate samples were run for the analysis of Au^{3+} and AuNPs at each time point. The data was reported as mean ± standard deviation.

Determination of AuNP Molarity. The calibration equation between the absorbance of AuNPs and corresponding molarity was built as follows. After Au^{3+} reduction by EPS, the suspensions were dialyzed for 48 h through a 3500 Da membrane (Viskase) to remove residual Au^{3+} (if any).[40] During the dialysis, dialysis water was changed every 6 h using fresh Milli-Q water. The resulting AuNPs in aqueous suspension were dried by evaporation at 105 °C, followed by digesting with 1 mL chloroazotic acid (HCl/HNO_3 = 3/1) at 105 °C. The concentration of Au^{3+} in the resulting solution was determined by iodometry.[41] In brief, the resulting solution was adjusted to pH 4.0 with 0.5 mol·L^{-1} NaOH, and titrated using an autotitrator (WDDY-2008J, Datang, China) equipped with an iodide ion electrode (PI-1−01, INESA, China) and a Ag/AgCl reference electrode (218, INESA, China). The titration was performed using 6.6 mol·L^{-1} KI at a speed of 10 μL per 20 s at 30 °C and 150 rpm stirring. The chemical reaction can be described as follows,

$$Au^{3+} + 2I^- = Au^+ + I_2 \quad (6)$$

According to the titration curve (SI Figure S2A), a linear relationship between AuNP absorbance ($OD_{524\ nm}$) and its molarity can be established as $[AuNPs] = 0.15 \times [OD_{524\ nm}] - 5.1 \times 10^{-3}$ over a range of 0.01−0.09 mmol·L^{-1}AuNPs (SI Figure S2B). The reliability of the iodometry method for Au^{3+} analysis was validated by inductively coupled plasma-atomic emission spectrometry (ICP-AES) (SI Figure S2C). In the present study, aggregation of AuNPs was minimal as reflected by the constant AuNP absorbance over a three-month storage.

DOI: 10.1021/acs.est.6b05930
Environ. Sci. Technol. 2017, 51, 2776−2785

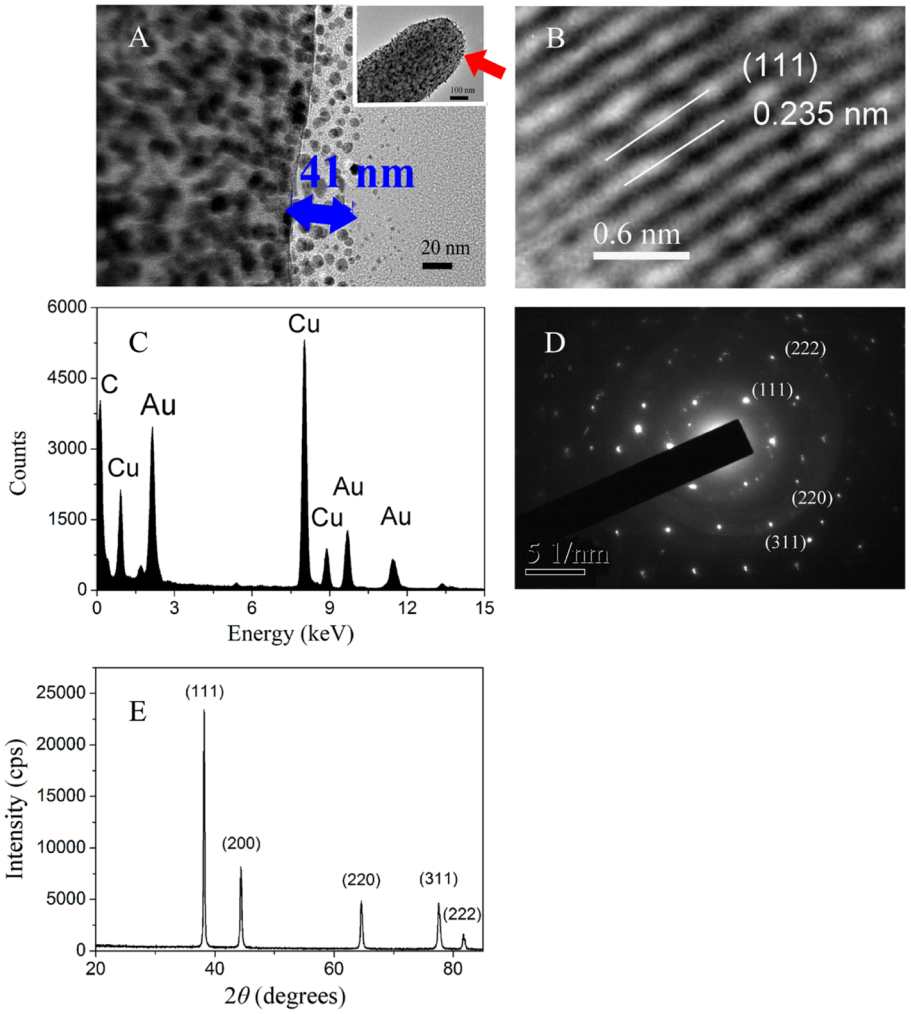

Figure 1. Microscopic and spectroscopic analyses of AuNPs formation from Au^{3+} (initially at 0.515 mmol·L^{-1}) on bacterial surface. (A) TEM images of AuNPs formed in the presence *E. coli* (9×10^{12} cells·L^{-1}). Red arrow points to *E. coli* cell coated with AuNPs, amplified on the left side. The AuNP accumulated EPS layer was about 41 nm thick (blue arrow). (B) HRTEM lattice-fringe fingerprinting of these AuNPs. The interplanar spacing (0.235 nm) is consistent with the crystal face of element gold. The corresponding characterization by EDS (C), SAED (D), and XRD (E). The signals of Cu and C in panel (C) originated from the carbon-coated copper grid.

Spectroscopic Analyses of AuNPs and EPS. A separate set of experiments was performed to produce AuNPs from Au^{3+} (initially 0.515 mmol·L^{-1}) in the presence of *E. coli* cells (9×10^{12} cells·L^{-1}) or aqueous dissolved EPS (32.8 mg·L^{-1} on a dry weight basis) for the purpose of structural characterization. After reduction reaction, the sample was freeze-dried (Labconco, UK). One portion of the pellet was placed onto a carbon-coated copper grid for imaging with high-resolution transmission electron microscopy (HRTEM) and selected area electron diffraction (SAED) (JEM-200CX, Horiba, Japan). Energy-dispersive spectroscopy (EDS) analysis was performed on the nanoparticles formed from Au^{3+} at 20 kV accelerating voltage and 133 eV resolution on a scanning area of 1×1 μm using an EX-250 spectrometer (Horiba, Japan). X-ray diffraction (XRD) patterns were recorded with an X'per PRO instrument (PANalytical, Almelo, Netherlands) using Cu Kα radiation (λ = 0.15418 nm) with the diffraction angle (2θ) at a range of 20−85°. X-ray photoelectron spectroscopy (XPS) analysis was performed on the nanoparticles at 30.0 eV pass energy in the broad survey scan and 70.0 eV pass energy in the high resolution scan using a PHI 5000 VersaProbe spectrometer (UlVAC-PHI, Japan). Particle size distributions of AuNPs mediated by *E. coil* cells, extracted EPS, and purified extracellular lipopolysaccharides were calculated based on the TEM images of at least 400 AuNP particles.

To identify the functional groups in EPS responsible for Au^{3+} reduction, XPS and Fourier transform infrared (FTIR) spectroscopy analyses were performed on EPS and/or lipopolysaccharides before and after reaction with Au^{3+}. The FTIR spectra of freeze-dried EPS/lipopolysaccharides mixed with KBr (mass ratio of 1:100) were acquired on a Nicolet NEXUS870 (Nicolet).

RESULTS AND DISCUSSION

Reduction of Au^{3+} in the Presence of *E. coli* or EPS. The formation of AuNPs was first examined by incubating the mixture of Au^{3+} and *E. coli* (9×10^{12} cells·L^{-1}) at the stable growth phase. TEM analysis showed noticeable amounts of nanoparticles were formed on the surface of *E. coli* cells after 6 h contact with Au^{3+} at 30 °C (Figure 1A). These nanoparticles were 2−15 nm in diameter with an average of 8 ± 3 nm (SI Figure S3), and occurred as mostly isolated particles within the EPS matrix on cell surfaces. The formation of AuNPs was verified by various microscopic and spectroscopic analyses. The

DOI: 10.1021/acs.est.6b05930
Environ. Sci. Technol. 2017, 51, 2776−2785

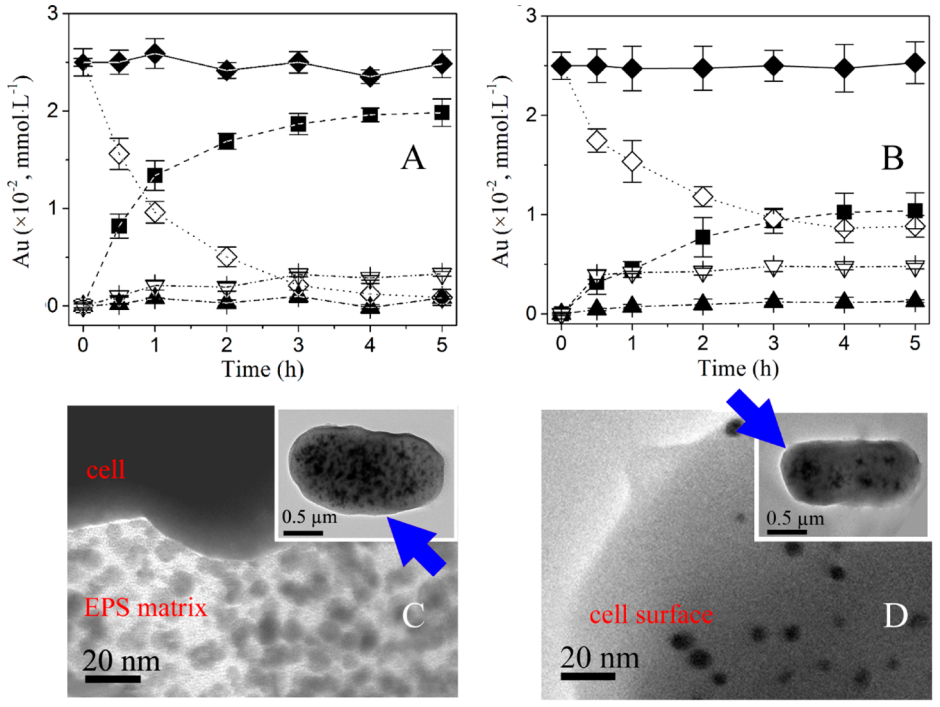

Figure 2. Extracellular formation of AuNPs from Au^{3+} (initially at 2.5×10^{-2} mmol·L^{-1}) in water suspension of *E. coli* (9×10^{12} cells·L^{-1}). Mass distribution of gold species in the presence of pristine *E. coli* cells without manipulation of EPS (A) or low-EPS *E. coli* cells with removal of EPS using the sonication/centrifugation method (B). ♦ mass balance, ◊ Au^{3+} outside cells, ▽ Au^{3+} inside cells, ■ AuNPs outside cells, ▲ AuNPs inside cells. TEM images of AuNPs formed on surface of pristine *E. coli* (C) and on surface of low-EPS *E. coli* (D). Blue arrows point to *E. coli* cells coated with AuNPs, amplified on the down side.

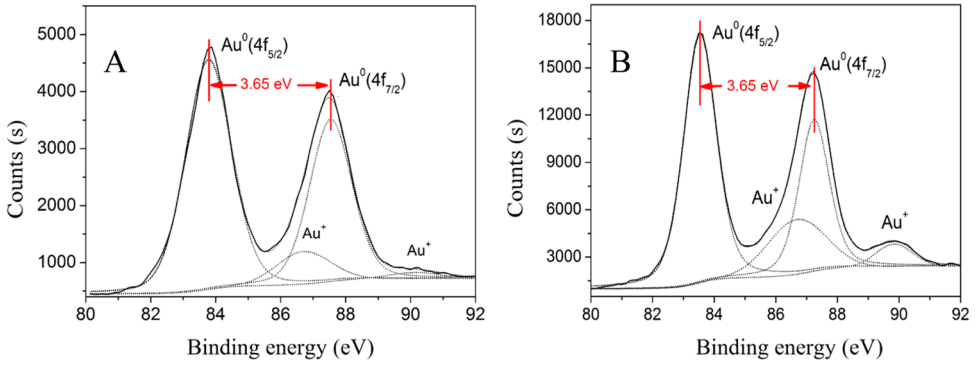

Figure 3. XPS analysis of AuNPs formed from the reduction of Au^{3+} in the presence of *E. coli* (9×10^{12} cells·L^{-1}) (A) or EPS (32.8 mg·L^{-1}) (B) for 6 h at 30 °C. Dash lines represent four components of peak fitting corresponding to Au^0 (87.5 and 83.8 eV) and Au^+ (86.7 and 89.9 eV). The amount of Au^+ accounts for 7.9% and 8.7% of the total Au in (A) and (B), respectively.

HRTEM image (Figure 1B) shows that the interplanar spacing of the lattice-fringe of the nanoparticles is 0.235 nm, consistent with the (111) lattice planes of metallic Au.[28,42] The EDS analysis suggests that the observed nanoparticles are largely comprised of Au (Figure 1C). The SAED and XRD analyses (Figure 1D, E) show the characteristic patterns associated with the (111), (200), (220), (311), and (222) atomic planes of metallic Au, indicating the formation of a face-centered cubic lattice.[43] No formation of AuNPs was observed in the absence of *E. coli* (control). These results collectively corroborate that Au^{3+}can be readily reduced on *E. coil* cell surfaces to AuNPs and accumulate within the extracellular matrix.

Figure 2A, B displays the mass distribution of gold species in *E. coli* water suspension as a function of incubation time. The recovery of total gold (i.e., mass balance) ranged from 92% to 101% for pristine *E. coli* and from 96% to 100% for low-EPS *E. coli*. For pristine *E. coli* cells, the concentration of Au^{3+} outside cells (i.e., in water and in extracellular matrix) gradually decreased from 2.5×10^{-2} to 1.1×10^{-3} mmol/L during the 5 h incubation period, whereas the concentration of AuNPs outside cells gradually increased from zero to 2.0×10^{-2} mmol/L (Figure 2A). The majority of AuNPs (95.2%) was formed outside *E. coli* cells. In contrast, the concentrations of Au^{3+} and AuNPs inside cells only slightly increased to 2.9×10^{-3} mmol/L and 1.5×10^{-3} mmol/L, respectively, which accounted for 11.6% and 6% of total gold. Compared with pristine *E. coli* cells, low-EPS *E. coli* cells exhibited similar mass distribution patterns of Au^{3+} and AuNPs, but with higher Au^{3+} concentrations (4.9×10^{-3} mol/L inside cells and 8.5×10^{-3} mmol/L outside cells) and lower outside-cell AuNP concentration (1.0×10^{-2} mmol/L) (Figure 2B). The TEM image analysis consistently showed that more AuNPs were coated on the pristine *E. coli* surface

DOI: 10.1021/acs.est.6b05930
Environ. Sci. Technol. 2017, 51, 2776−2785

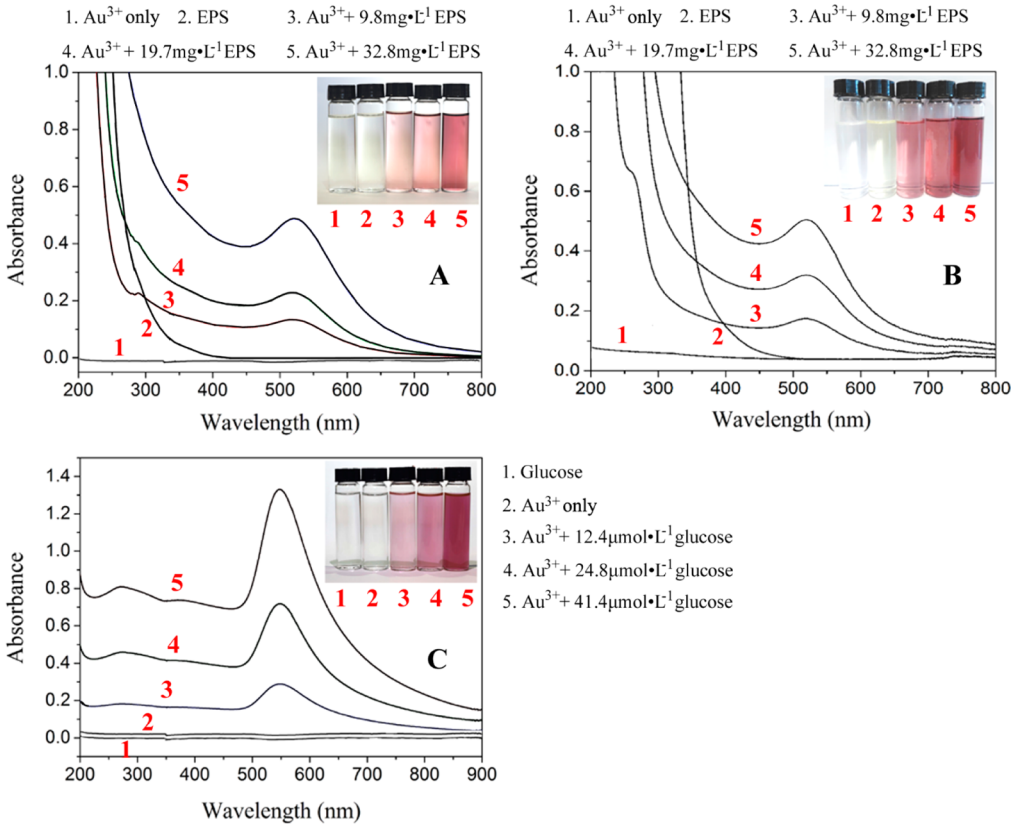

Figure 4. In vitro formation of AuNPs from Au^{3+} (initially at 0.515 mmol·L^{-1}) characterized by UV−vis absorbance spectra and photographing at various concentrations of EPS at pH 7.2 (A) and at extreme alkaline pH 13.8 (B) or D-glucose at pH 7.2 (C) The reaction mixture was incubated at 30 °C for 6 h. The initial concentration of Au^{3+}, if added, was 0.515 mmol·L^{-1}.

than on the low-EPS *E. coli* surface (Figure 2C, D). After the removal of EPS, pronouncedly less Au^{3+} was reduced to AuNPs and more Au^{3+} penetrated into *E. coli* cells. Nonetheless, the formation of AuNPs inside low-EPS *E. coli* cells was minimal (up to 4.8% of total gold). These results unambiguously demonstrate that the reduction of Au^{3+} to AuNPs was dominated by the extracellular matrix.

To better understand the role of EPS in the extracellular formation of AuNPs, Au^{3+} was incubated with extracted *E. coli* EPS (cell-free) at 30 °C. As shown in SI Figure S3 and Figure S4A, nanoparticles with similar size and shape as those observed on *E. coli* cells were generated in vitro in the presence of only EPS. These nanoparticles were verified to be AuNPs by spectroscopic analyses including HRTEM (SI Figure S4B), EDS (SI Figure S4C), SAED (SI Figure S4D), and XRD (SI Figure S4E). Thus, EPS alone can mediate the reductive formation of AuNPs.

The speciation of Au during the reduction process was further investigated using XPS. Figure 3 shows the XPS spectra of AuNPs formed in the presence of *E. coli* or aqueous dissolved EPS. There were two prominent peaks at 87.5 and 83.8 eV, which correspond to the Au $4f_{7/2}$ and Au $4f_{5/2}$ signals of metallic (zerovalent) Au, corroborating the formation of AuNPs.[44] Furthermore, two characteristic peaks of Au^{+} were also observed at 86.7 and 89.9 eV.[40] The results indicate that Au^{+} was the intermediate species during the formation process of AuNPs.[45]

After 6 h incubation, the characteristic peak of the surface plasmon resonance (SPR) of AuNPs at 524 nm[46] was observed in the presence of EPS (Figure 4A). Consistently, the color of the mixture of EPS and Au^{3+} gradually changed from clear to ruby red during the incubation. The intensity of SPR can be used to quantify the generation of AuNPs.[47] Figure 4A shows that the intensity of SPR increased with increasing EPS concentration, indicating that the formation rate of AuNPs increased with the EPS concentration. The high consistency of spectroscopic fingerprint of *E. coli*- and EPS-mediated AuNPs, as well as the dependence of reaction kinetics on the EPS concentration collectively indicates that EPS played a critical role in the reductive formation of AuNPs in the *E. coli* suspension. Furthermore, EPS could effectively reduce Au^{3+} to AuNPs at very high pH (13.8) (Figure 4B). This rules out the possibility of Au^{3+} reduction by reduced extracellular enzymes, which if present should have been deactivated under such extreme alkaline conditions.[48,49] It is noteworthy that changing EPS concentration or pH only slightly affected the particle size distribution of AuNPs (SI Figure S3). Compared to the relatively high toxicity of Au^{3+}, the toxicity of AuNPs formed in vitro in the presence of EPS is minimal, as indicated by the *E. coli* growth tests (SI Figure S5). Therefore, EPS act as a permeability barrier to antagonize the toxicity of Au^{3+} to microbes.

Identification of EPS Reducing Agents Responsible for Au^{3+} Reduction. Although Au^{3+} reduction by various microbes has been reported,[25,28,50] the underlying mechanism, particularly the reducing agents involved are not well understood. Previous studies reported that the peptide/protein thiol groups may serve as the reducing agent responsible for Au^{3+} reduction.[28] However, this mechanism can be ruled out by the fact that the sulfur content in the tested EPS was too low

DOI: 10.1021/acs.est.6b05930
Environ. Sci. Technol. 2017, 51, 2776−2785

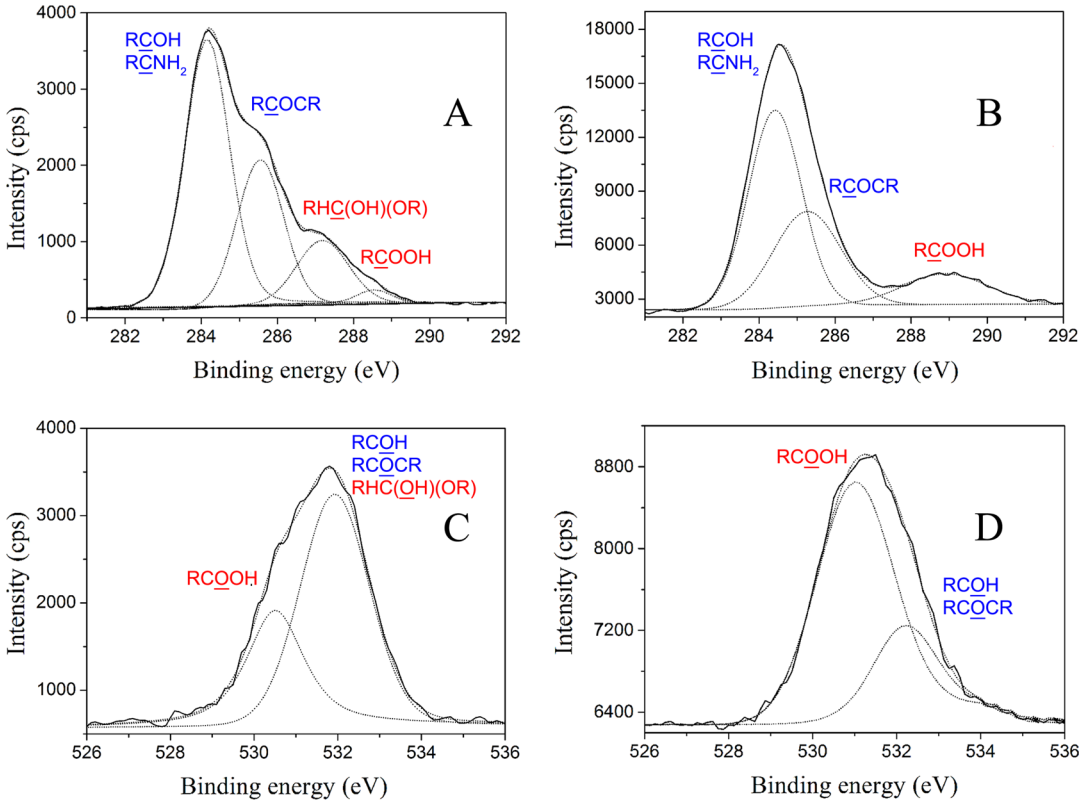

Figure 5. Comparison of XPS signals of EPS (initially at 32.8 mg·L^{-1}) before and after reacting with Au^{3+} (initially at 0.515 mmol·L^{-1}) for 6 h at 30 °C. (A) C 1s signals of pristine EPS. (B) C 1s signals of EPS after reaction. (C) O 1s signals of pristine EPS. (D) O 1s signals of EPS after reaction. *R* represents substituent groups associated with other chain of polysaccharides, lipids or protein-like structures. For the C 1s signals in (A) and (B), hydroxyl (RCOH)/amino ($RCNH_2$): 284.2 eV; glucoside (RCOCR): 285.6 eV; hemiacetal (RHC(OH) (OR)): 287.5 eV; carboxylate (RCOOH): 288.7 eV. For the O 1s signals in (C) and (D), RCOOH: 530.6 eV; RCOH, RCOCR, and RHC(OH) (OR): 532.2 eV.

(0.49% in *E. coli* EPS)[33] to produce AuNPs of the measured amount. Assuming that all sulfur in EPS exists as thiol groups and all thiol groups are converted to elemental sulfur, the maximum amount of electrons donated can only account for 5.3% of the stoichiometric electron consumption to reduce Au^{3+}. We show herein the involvement of hemiacetal groups of EPS in Au^{3+} reduction by comparing XPS spectra of EPS before and after reaction with Au^{3+} (Figure 5). XPS analysis has been used to characterize carbohydrates as well as their structural changes induced by redox reactions.[51] For pristine EPS, the C 1s peak at 284.3 eV corresponds to hydroxyl (RCOH) or amino ($RCNH_2$) carbon atoms,[43,52,53] other peaks at 285.6, 287.5, and 288.7 eV can be ascribed to carbon atoms of glucoside (RCOCR), hemiacetal (RHC(OH) (OR)), and carboxylate (RCOOH),[42,44,54] respectively. After reaction with Au^{3+}, a substantial decrease of the RHC(OH) (OR) signal (287.5 eV) and a simultaneous increase in the RCOOH signal (288.7 eV) were observed (Figure 5A, B). This indicates that the hemiacetal groups of saccharides in EPS were oxidized during the reaction with Au^{3+}. In contrast, the C 1s signals of hydroxyl/amino (284.3 ev) and gluocoside (285.6 eV) kept nearly constant, suggesting that these groups were not involved in the reaction. The O 1s signal at 530.6 eV can be assigned to RCOOH, and the signal at 532.2 eV can be assigned to RCOH, RCOCR, and RHC(OH) (OR) of saccharides[44] (Figure 5C). After reaction with Au^{3+} the carboxylate O 1s signal (530.6 eV) increased while the superposed saccharide signal (532.2 eV) decreased (Figure 5D). Accordingly, the hemiacetal groups of saccharides serve as the reducing agents responsible for Au^{3+} reduction in the presence of EPS.

The reducing capability of polysaccharides in EPS was further supported by the evidence that purified *E. coli* extracellular lipopolysaccharides could reduce Au^{3+} to AuNPs, as confirmed by spectroscopic analyses including HRTEM, EDS, SAED, and XRD (SI Figure S6), as well as particle size distribution analysis (SI Figure S3). Consistently, comparison of FTIR spectra of EPS and purified extracellular lipopolysacchrides before and after reaction with Au^{3+} indicates that the hemiacetal groups of saccharides (corresponding to the peaks at 1080−1240 cm^{-1}) were oxidized to carboxyl groups (peak at 1451 cm^{-1}) (SI Figure S7). Notably, the purified lipopolysaccharides contained negligible sulfur (<0.08%), ruling out the possibility again that the reduction of Au^{3+} was induced by reducing sulfide groups (e.g., thiols) in peptides and proteins. Overall, these results demonstrate that Au^{3+} can be reduced to AuNPs (with Au^{+} as an intermediate) by the hemiacetal groups (aldehyde equivalents) in EPS. The reaction pathway can be described as follows:

$$RCHO + Au^{3+} = RCOOH + Au^{+} \quad (7)$$

$$RCHO + 2Au^{+} = RCOOH + 2Au \quad (8)$$

To further confirm this hypothesis, D-glucose with hemiacetal groups was employed as a surrogate of reducing saccharides in EPS. Figure 4C shows a dose-dependent formation of AuNPs from the reduction of Au^{3+} by hemiacetal groups of D-glucose. These nanoparticles were slightly larger (3−19 nm in size) than those generated in the presence of *E. coli* cells or EPS (2−15

DOI: 10.1021/acs.est.6b05930
Environ. Sci. Technol. 2017, 51, 2776−2785

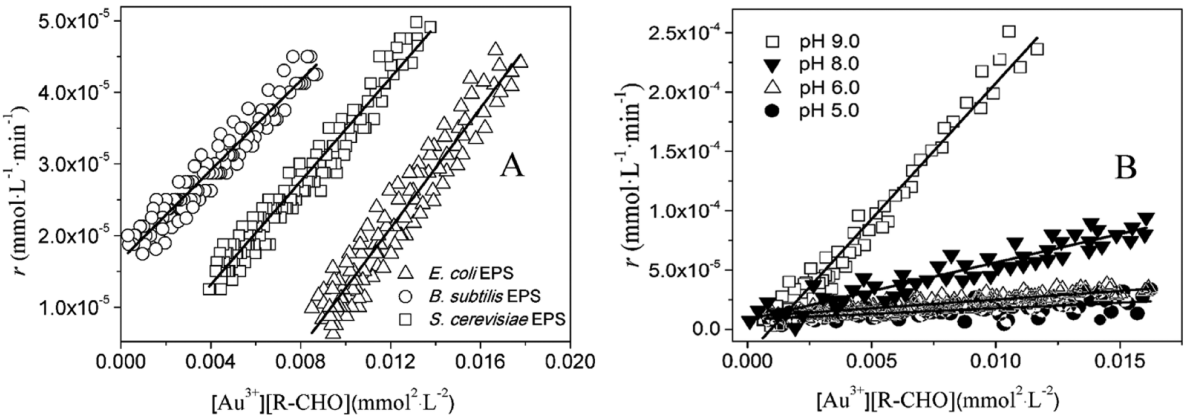

Figure 6. Hemiacetal-dependent reduction kinetics of Au^{3+} (initially at 0.515 mmol·L^{-1}) in aqueous dissolved EPS separated from different microbes (*E. coli*, *B. subtilis*, and *S. cerevisiae*) (A) and pH effects on reaction kinetics mediated by *E. coli* EPS (B). Pseudo-second-order kinetics plotted as *r* against [Au^{3+}][R-CHO]; *r* represents the reaction rate, and [Au^{3+}][R-CHO] is the product of molarities of Au^{3+} and R-CHO (hemiacetal groups) in EPS. The reaction rate constants (reported as means ± standard deviations) in (A) are (4.2 ± 0.1) × 10^{-3} (*E. coli* EPS, R^2 = 0.93), (3.13 ± 0.08) × 10^{-3} (*B. subtilis* EPS, R^2 = 0.96), and (3.61 ± 0.07) × 10^{-3} $mmol^{-1}$·L·min^{-1} (*S. cerevisiae* EPS, R^2 = 0.92); the reaction rate constants in (B) are (2.3 ± 0.1) × 10^{-2} (pH 9.0, R^2 = 0.97), (4.82 ± 0.03) × 10^{-3} (pH 8.0, R^2 = 0.89), (1.5 ± 0.2) × 10^{-3} $mmol^{-1}$·L·min^{-1} (pH 6.0, R^2 = 0.79), and (9.46 ± 0.03) × 10^{-4} (pH 5.0, R^2 = 0.70).

nm) (SI Figure S3). As the concentration of D-glucose increased from 0 to 0.515 mmol·L^{-1}, the maximum UV−vis absorbance of AuNPs (at 542 nm)[55] gradually increased from 0 to 1.32. Accordingly, the color of the mixture changed from clear to ruby red, similar to that observed in reaction with EPS. These results corroborate the critical role of hemiacetal groups in formation of AuNPs in aqueous dissolved EPS or on microbial cell surfaces.

Au^{3+} Reduction Kinetics As Affected by Microbial Sources of EPS and pH. The formation kinetics of AuNPs from Au^{3+} was quantified in the presence of EPS (initially at 32.8 mg·L^{-1}) extracted from different microbes (i.e., Gram-negative *E. coli*, Gram-positive *B. subtilis*, and fungal *S. cerevisiae*) (Figure 6A). The AuNPs formed in the presence of three different microbial EPS exhibited similar distribution patterns of particle size with averages of 7.4−7.7 nm (SI Figure S3). The concentration of AuNPs, formation rate of AuNPs (mmol·L·min^{-1}), concentration of Au^{3+}, and concentration of hemiacetal groups as a function of time were measured to calculate the reaction kinetics using EPS originated from these three different microbes (SI Figure S8). The concentrations of reactants including oxidant Au^{3+} and reductants in the three EPS gradually decreased as the concentration of AuNPs increased. The formation rate of AuNPs (*r*) can be well described by the pseudo-second-order kinetic model (with regression coefficient R^2 > 0.92):

$$r = k_2[Au^{3+}][R - CHO] \quad (9)$$

where k_2 is the observed pseudo-second-order rate constant ($mmol^{-1}$·L·min^{-1}), and [Au^{3+}] and [R-CHO] are the molarities (mmol·L^{-1}) of Au^{3+} and R-CHO (hemiacetal groups), respectively. The hemiacetal-dependent reduction kinetics of Au^{3+} in the presence of different microbial EPS is presented in Figure 6A. The rate constant k_2 for reaction kinetics is (4.2 ± 0.1)× 10^{-3} $mmol^{-1}$·L·min^{-1} (R^2 = 0.93, P > 0.01) for *E. coli* EPS, (3.13 ± 0.08) × 10^{-3} $mmol^{-1}$·L·min^{-1} (R^2 = 0.96, P > 0.01) for *B. subtilis* EPS, and (3.61 ± 0.07)× 10^{-3} $mmol^{-1}$·L·min^{-1} (R^2 = 0.92, P > 0.05) for *S. cerevisiae* EPS. It is worth noting that those rate constants are very close although the EPS extracted from the three microbes have very different structural components, such as the content of O-containing functionalities.[53,56] Given the same initial Au^{3+} concentration (0.515 mmol·L^{-1}), the reduction rate is mainly controlled by the concentration of hemiacetal groups in EPS regardless of their microbial origin. The reaction kinetics analysis confirms that the hemiacetal groups of reducing saccharides in EPS serve as the reducing agents for Au^{3+} reduction.

The observed pH dependence of Au^{3+} reduction kinetics (Figure 6B) also suggests that the reaction is dominated by the hemiacetal groups of reducing saccharides. As the pH was increased from 5.0 to 9.0, the rate constant k_2 increased by more than 1 order of magnitude from 9.46 × 10^{-4} to 2.3 × 10^{-2} mmol·L^{-1}·min^{-1}. It has been reported that hydroxyl ions catalyze the nucleophilic addition reaction of aldehyde groups in Tollen's reaction.[57] Additionally, the hemiacetal-dependent reduction kinetics of Au^{3+} in the presence of purified *E. coli* extracellular lipopolysaccharides (SI Figure S9) reaffirms the key role played by reducing extracellular saccharides in the reaction. The rate constant k_2 for reaction kinetics is (4.14 ± 0.02) × 10^{-3} mmol·L^{-1}·min^{-1} (R^2 = 0.99, P > 0.01) for lipopolysaccharides, which is very close to the measured rate constants for the three EPS.

Environmental Implications. Considering their environmental abundance and ubiquity (i.e., up to 50% of the labile and semilabile dissolved organic matter in natural waters[11]), EPS might play an important and previously overlooked role in the biomineralization of Au and possibly other metals, influencing their biogeochemical cycling, fate, and potential toxicity. A recent study suggests that DOM can mediate the reduction of Ag^+ and Au^{3+} to metallic nanoparticles through sunlight-induced generation of superoxide.[36] In the present study, we first demonstrate that EPS produced by common microorganisms that are not known for reducing metals for metabolic (respiration) purposes can chemically change the metal speciation into zerovalent nanoparticles, using saccharides as reducing agents without the assistance of light or enzymes. Our study expands the quantitative understanding of the environmental and geochemical importance of EPS by highlighting its critical role in the reduction process of high-oxidation-state metal species.

DOI: 10.1021/acs.est.6b05930
Environ. Sci. Technol. 2017, 51, 2776−2785

Reducing saccharides can be found in many biological systems besides microbial EPS, including plant tissues and their extracts. Thus, they could also be responsible for the reported biomineralization of Au in plants.[58−61] Consistently, earlier studies demonstrated that Au^{3+} can be reduced to AuNPs in plant tissues such as alfalfa shoot biomass[62] and Sesbania seedlings.[58] Our study suggests a possibility that these reduction processes are related to abundant saccharides in higher plants. This underscores the need for further research to understand the broader environmental and geochemical significance of reducing saccharides in biogeochemical cycles of heavy metals and also in the context of natural attenuation of other oxidized chemicals of concern in the environment.

■ ASSOCIATED CONTENT

Supporting Information

The Supporting Information is available free of charge on the ACS Publications website at DOI: 10.1021/acs.est.6b05930.

Titration curves of residual Ag^+ by Cl^- (Figure S1); relationship of the absorbance ($OD_{524\ nm}$) and molarity of AuNPs (Figure S2); particle size distributions of AuNPs formed under different conditions (Figure S3); microscopic and spectroscopic analyses of AuNPs formed in vitro from Au^{3+} in the presence of aqueous *E. coli* EPS (Figure S4) and aqueous extracted lipopolysaccharides (Figure S6); toxicity test of Au^{3+} and AuNPs on *E. coli* growth (Figure S5); comparison of FTIR spectra of EPS/lipopolysaccharides before and after reaction with Au^{3+} (Figure S7); concentration of AuNPs, formation rate of AuNPs, concentration of Au^{3+}, and concentration of hemiacetal groups as a function of time for EPS originated from three different microbes (Figure S8); the hemiacetal-dependent reduction kinetics of Au^{3+} in the presence of aqueous extracted lipopolysaccharides (Figure S9) (PDF)

■ AUTHOR INFORMATION

Corresponding Author

*Phone/fax: +86 (010) 62766405; e-mail: zhud@pku.edu.cn.

ORCID

Pedro J. J. Alvarez: 0000-0002-6725-7199

Dongqiang Zhu: 0000-0001-6190-5522

Notes

The authors declare no competing financial interest.

■ ACKNOWLEDGMENTS

This work was supported by the National Key Basic Research Program of China (Grant 2014CB441103), the National Natural Science Foundation of China (Grants 21237002, 21225729, 21428701, 41401543, and 2014M561662), the National Science Foundation for Postdoctoral Scientists of China (Grant 2014M561662), the Natural Science Foundation of Jiangsu Province of China (Grant BK20140725), and the Fundamental Research Funds for the Central Universities (Grant KJQN201518). This work was also partially supported by the NSF Engineering Research Center on Nanotechnology-Enabled Water Treatment (Grant EEC-1449500).

■ REFERENCES

(1) Lowenstam, H. A. Minerals formed by organisms. *Science* **1981**, *211* (4487), 1126−1131.

(2) Douglas, S.; Beveridge, T. J. Mineral formation by bacteria in natural microbial communities. *FEMS Microbiol. Ecol.* **1998**, *26* (2), 79−88.

(3) Ghiorse, W. Biology of iron-and manganese-depositing bacteria. *Annu. Rev. Microbiol.* **1984**, *38* (1), 515−550.

(4) Lovley, D. R.; Roden, E. E.; Phillips, E.; Woodward, J. Enzymatic iron and uranium reduction by sulfate-reducing bacteria. *Mar. Geol.* **1993**, *113* (1), 41−53.

(5) Shen, H.; Wang, Y. Characterization of enzymatic reduction of hexavalent chromium by *Escherichia coli* ATCC 33456. *Appl. Environ. Microb.* **1993**, *59* (11), 3771−3777.

(6) Islam, F. S.; Gault, A. G.; Boothman, C.; Polya, D. A.; Charnock, J. M.; Chatterjee, D.; Lloyd, J. R. Role of metal-reducing bacteria in arsenic release from Bengal delta sediments. *Nature* **2004**, *430* (6995), 68−71.

(7) Sani, R. K.; Peyton, B. M.; Amonette, J. E.; Geesey, G. G. Reduction of uranium (VI) under sulfate-reducing conditions in the presence of Fe (III)-(hydr) oxides. *Geochim. Cosmochim. Acta* **2004**, *68* (12), 2639−2648.

(8) Fredrickson, J. K.; Gorby, Y. A. Environmental processes mediated by iron-reducing bacteria. *Curr. Opin. Biotechnol.* **1996**, *7* (3), 287−294.

(9) Sutherland, I. W. The biofilm matrix−an immobilized but dynamic microbial environment. *Trends Microbiol.* **2001**, *9* (5), 222−227.

(10) Flemming, H.-C.; Wingender, J. The biofilm matrix. *Nat. Rev. Microbiol.* **2010**, *8* (9), 623−633.

(11) Bhaskar, P.; Bhosle, N. B. Microbial extracellular polymeric substances in marine biogeochemical processes. *Curr. Sci.* **2005**, *88* (1), 45−53.

(12) Vu, B.; Chen, M.; Crawford, R. J.; Ivanova, E. P. Bacterial extracellular polysaccharides involved in biofilm formation. *Molecules* **2009**, *14* (7), 2535−2554.

(13) Teitzel, G. M.; Parsek, M. R. Heavy metal resistance of biofilm and planktonic *Pseudomonas aeruginosa*. *Appl. Environ. Microb.* **2003**, *69* (4), 2313−2320.

(14) Kenney, J. P.; Fein, J. B. Importance of extracellular polysaccharides on proton and Cd binding to bacterial biomass: A comparative study. *Chem. Geol.* **2011**, *286* (3), 109−117.

(15) Chan, C. S.; De Stasio, G.; Welch, S. A.; Girasole, M.; Frazer, B. H.; Nesterova, M. V.; Fakra, S.; Banfield, J. F. Microbial polysaccharides template assembly of nanocrystal fibers. *Science* **2004**, *303* (5664), 1656−1658.

(16) Moreau, J. W.; Weber, P. K.; Martin, M. C.; Gilbert, B.; Hutcheon, I. D.; Banfield, J. F. Extracellular proteins limit the dispersal of biogenic nanoparticles. *Science* **2007**, *316* (5831), 1600−1603.

(17) Harish, R.; Samuel, J.; Mishra, R.; Chandrasekaran, N.; Mukherjee, A. Bio-reduction of Cr(VI) by exopolysaccharides (EPS) from indigenous bacterial species of Sukinda chromite mine, India. *Biodegradation* **2012**, *23* (4), 487−496.

(18) Cao, B.; Ahmed, B.; Kennedy, D. W.; Wang, Z.; Shi, L.; Marshall, M. J.; Fredrickson, J. K.; Isern, N. G.; Majors, P. D.; Beyenal, H. Contribution of extracellular polymeric substances from *Shewanella sp.* HRCR-1 biofilms to U(VI) immobilization. *Environ. Sci. Technol.* **2011**, *45* (13), 5483−5490.

(19) Kang, F.; Alvarez, P. J.; Zhu, D. Microbial extracellular polymeric substances reduce Ag^+ to silver nanoparticles and antagonize bactericidal activity. *Environ. Sci. Technol.* **2013**, *48* (1), 316−322.

(20) Srivastava, S. K.; Yamada, R.; Ogino, C.; Kondo, A. Biogenic synthesis and characterization of gold nanoparticles by *Escherichia coli* K12 and its heterogeneous catalysis in degradation of 4-nitrophenol. *Nanoscale Res. Lett.* **2013**, *8* (1), 2−9.

(21) Schröfel, A.; Kratošová, G.; Bohunická, M.; Dobročka, E.; Vávra, I. Biosynthesis of gold nanoparticles using diatoms—silica-gold and EPS-gold bionanocomposite formation. *J. Nanopart. Res.* **2011**, *13* (8), 3207−3216.

(22) Dahoumane, S. A.; Djediat, C.; Yéprémian, C.; Couté, A.; Fiévet, F.; Coradin, T.; Brayner, R. Species selection for the design of gold

nanobioreactor by photosynthetic organisms. *J. Nanopart. Res.* **2012**, *14* (6), 1−17.
(23) Kenney, J. P.; Song, Z.; Bunker, B. A.; Fein, J. B. An experimental study of Au removal from solution by non-metabolizing bacterial cells and their exudates. *Geochim. Cosmochim. Acta* **2012**, *87*, 51−60.
(24) Beattie, I. R.; Haverkamp, R. G. Silver and gold nanoparticles in plants: Sites for the reduction to metal. *Metallomics* **2011**, *3* (6), 628−632.
(25) Ahmad, A.; Senapati, S.; Khan, M. I.; Kumar, R.; Sastry, M. Extracellular biosynthesis of monodisperse gold nanoparticles by a novel extremophilic actinomycete, *Thermomonospora sp. Langmuir* **2003**, *19* (8), 3550−3553.
(26) Mukherjee, P.; Senapati, S.; Mandal, D.; Ahmad, A.; Khan, M. I.; Kumar, R.; Sastry, M. Extracellular synthesis of gold nanoparticles by the fungus *Fusarium oxysporum*. *ChemBioChem* **2002**, *3* (5), 461−463.
(27) Reith, F.; Lengke, M. F.; Falconer, D.; Craw, D.; Southam, G. The geomicrobiology of gold. *ISME J.* **2007**, *1* (7), 567−584.
(28) Gardea-Torresdey, J.; Tiemann, K.; Gamez, G.; Dokken, K.; Cano-Aguilera, I.; Furenlid, L. R.; Renner, M. W. Reduction and accumulation of gold (III) by *Medicago sativa alfalfa* biomass: X-ray absorption spectroscopy, pH, and temperature dependence. *Environ. Sci. Technol.* **2000**, *34* (20), 4392−4396.
(29) Johnston, C. W.; Wyatt, M. A.; Li, X.; Ibrahim, A.; Shuster, J.; Southam, G.; Magarvey, N. A. Gold biomineralization by a metallophore from a gold-associated microbe. *Nat. Chem. Biol.* **2013**, *9* (4), 241−243.
(30) Pontel, L. B.; Audero, M. E. P.; Espariz, M.; Checa, S. K.; Soncini, F. C. GolS controls the response to gold by the hierarchical induction of Salmonella-specific genes that include a CBA efflux-coding operon. *Mol. Microbiol.* **2007**, *66* (3), 814−825.
(31) Kundu, S.; Pal, A.; Ghosh, S. K.; Nath, S.; Panigrahi, S.; Praharaj, S.; Pal, T. A new route to obtain shape-controlled gold nanoparticles from Au (III)-β-diketonates. *Inorg. Chem.* **2004**, *43* (18), 5489−5491.
(32) Johnson, C. J.; Dujardin, E.; Davis, S. A.; Murphy, C. J.; Mann, S. Growth and form of gold nanorods prepared by seed-mediated, surfactant-directed synthesis. *J. Mater. Chem.* **2002**, *12* (6), 1765−1770.
(33) Kang, F.; Zhu, D. Abiotic reduction of 1, 3-dinitrobenzene by aqueous dissolved extracellular polymeric substances produced by microorganisms. *J. Environ. Qual.* **2013**, *42* (5), 1441−1448.
(34) Dubois, M.; Gilles, K. A.; Hamilton, J. K.; Rebers, P.; Smith, F. Colorimetric method for determination of sugars and related substances. *Anal. Chem.* **1956**, *28* (3), 350−356.
(35) Burton, K. A study of the conditions and mechanism of the diphenylamine reaction for the colorimetric estimation of deoxyribonucleic acid. *Biochem. J.* **1956**, *62* (2), 315−318.
(36) Lowry, O. H.; Rosebrough, N. J.; Farr, A. L.; Randall, R. J. Protein measurement with the Folin phenol reagent. *J. Biol. Chem.* **1951**, *193* (1), 265−275.
(37) Siggia, S.; Segal, E. Determination of aldehydes in presence of acids, ketones, acetals, and vinyl ethers. *Anal. Chem.* **1953**, *25* (4), 640−642.
(38) Cromwell, N. H.; Tsou, K. C. Keto-hemiacetal tautomerism of some N-phenacyl-N-substituted ethanolamines. *J. Am. Chem. Soc.* **1949**, *71* (3), 993−996.
(39) Khym, J. X.; Cohn, W. E. Characterizations and some chemical reactions of periodate-oxidized nucleosides. *J. Am. Chem. Soc.* **1960**, *82* (24), 6380−6386.
(40) Yin, Y.; Liu, J.; Jiang, G. Sunlight-induced reduction of ionic Ag and Au to metallic nanoparticles by dissolved organic matter. *ACS Nano* **2012**, *6* (9), 7910−7919.
(41) Marczenko, Z.; Jankowski, K. Sensitive flotation-spectrophotometric determination of gold, based on the gold(I)-iodide-methylene blue system. *Talanta* **1985**, *32* (4), 291−294.
(42) Gardea-Torresdey, J.; Parsons, J.; Gomez, E.; Peralta-Videa, J.; Troiani, H.; Santiago, P.; Yacaman, M. J. Formation and growth of Au nanoparticles inside live alfalfa plants. *Nano Lett.* **2002**, *2* (4), 397−401.
(43) Yin, Y.; Y, S.; Liu, J.; Jiang, G. Thermal and photoinduced reduction of ionic Au(III) to elemental Au nanoparticles by dissolved organic matter in water: Possible source of naturally occurring Au nanoparticles. *Environ. Sci. Technol.* **2014**, *48* (5), 2671−2679.
(44) Wagner, C. D. *Handbook of X-ray Photoelectron Spectroscopy: A Reference Book of Standard Data for Use in X-Ray Photoelectron Spectroscopy*; Physical Electronics Division, Perkin-Elmer Corp., 1979.
(45) Reith, F.; Etschmann, B.; Grosse, C.; Moors, H.; Benotmane, M. A.; Monsieurs, P.; Grass, G.; Doonan, C.; Vogt, S.; Lai, B. Mechanisms of gold biomineralization in the bacterium *Cupriavidus metallidurans*. *Proc. Natl. Acad. Sci. U. S. A.* **2009**, *106* (42), 17757−17762.
(46) Thomas, M.; Klibanov, A. M. Conjugation to gold nanoparticles enhances polyethylenimine's transfer of plasmid DNA into mammalian cells. *Proc. Natl. Acad. Sci. U. S. A.* **2003**, *100* (16), 9138−9143.
(47) Hartmann, G.; Schuster, M. Species selective preconcentration and quantification of gold nanoparticles using cloud point extraction and electrothermal atomic absorption spectrometry. *Anal. Chim. Acta* **2013**, *761*, 27−33.
(48) Mozhaev, V.; Martinek, K. Inactivation and reactivation of proteins (enzymes). *Enzyme Microb. Technol.* **1982**, *4* (5), 299−309.
(49) Hass, L.; Lewis, M. Alkali-induced structural changes in muscle aldolase. *Biochemistry* **1963**, *2* (6), 1368−1376.
(50) Ogi, T.; Saitoh, N.; Nomura, T.; Konishi, Y. Room-temperature synthesis of gold nanoparticles and nanoplates using *Shewanella* algae cell extract. *J. Nanopart. Res.* **2010**, *12* (7), 2531−2539.
(51) Stevens, J. S.; Schroeder, S. L. Quantitative analysis of saccharides by X-ray photoelectron spectroscopy. *Surf. Interface Anal.* **2009**, *41* (6), 453−462.
(52) Xu, Z.; Uddin, K. M. A.; Kamra, T.; Schnadt, J.; Ye, L. Fluorescent boronic acid polymer grafted on silica particles for affinity separation of saccharides. *ACS Appl. Mater. Interfaces* **2014**, *6* (3), 1406−1414.
(53) László, K.; Tombácz, E.; Josepovits, K. Effect of activation on the surface chemistry of carbons from polymer precursors. *Carbon* **2001**, *39* (8), 1217−1228.
(54) De'Nève, B.; Delamar, M.; Nguyen, T.; Shanahan, M. Failure mode and ageing of steel/epoxy joints. *Appl. Surf. Sci.* **1998**, *134* (1), 202−212.
(55) Haiss, W.; Thanh, N. T.; Aveyard, J.; Fernig, D. G. Determination of size and concentration of gold nanoparticles from UV-vis spectra. *Anal. Chem.* **2007**, *79* (11), 4215−4221.
(56) Černá, M.; Barros, A. S.; Nunes, A.; Rocha, S. M.; Delgadillo, I.; Čopíková, J.; Coimbra, M. A. Use of FT-IR spectroscopy as a tool for the analysis of polysaccharide food additives. *Carbohydr. Polym.* **2003**, *51* (4), 383−389.
(57) Benet, W. E.; Lewis, G. S.; Yang, L. Z.; Hughes, P. D. The mechanism of the reaction of the Tollens reagent. *J. Chem. Res.* **2011**, *35* (12), 675−677.
(58) Sharma, N. C.; Sahi, S. V.; Nath, S.; Parsons, J. G.; Gardea-Torresde, J. L.; Pal, T. Synthesis of plant-mediated gold nanoparticles and catalytic role of biomatrix-embedded nanomaterials. *Environ. Sci. Technol.* **2007**, *41* (14), 5137−5142.
(59) Armendariz, V.; Herrera, I.; Jose-yacaman, M.; Troiani, H.; Santiago, P.; Gardea-Torresdey, J. L. Size controlled gold nanoparticle formation by Avena sativa biomass: Use of plants in nano-biotechnology. *J. Nanopart. Res.* **2004**, *6* (4), 377−382.
(60) Marshall, A. T.; Haverkamp, R. G.; Davies, C. E.; Parsons, J. G.; Gardea-Torresdey, J. L.; van Agterveld, D. Accumulation of gold nanoparticles in Brassic juncea. *Int. J. Phytorem.* **2007**, *9* (3), 197−206.
(61) Rodriguez, E.; Parsons, J. G.; Peralta-Videa, J. R.; Cruz-Jimenez, G.; Romero-Gonzalez, J.; Sanchez-Salcido, B. E.; Saupe, G. B.; Duarte-Gardea, M.; Gardea-Torresdey, J. L. Potential of *Chilopsis linearis* for gold phytomining: Using XAS to determine gold reduction and nanoparticle formation within plant tissues. *Int. J. Phytorem.* **2007**, *9* (2), 133−147.
(62) Shankar, S. S.; Rai, A.; Ahmad, A.; Sastry, M. Rapid synthesis of Au, Ag, and bimetallic Au core-Ag shell nanoparticles using Neem (*Azadirachta indica*) leaf broth. *J. Colloid Interface Sci.* **2004**, *275* (2), 496−502.

DOI: 10.1021/acs.est.6b05930
Environ. Sci. Technol. 2017, 51, 2776−2785